Chapter 6

Thermal Stability of Ultra-Fine Grained Microstructure in Mg and Ti Alloys

Jitka Stráská, Pavel Zháňal, Kristína Václavová, Josef Stráský, Petr Harcuba, Jakub Čížek and Miloš Janeček

Additional information is available at the end of the chapter

http://dx.doi.org/10.5772/intechopen.68956

Abstract

This chapter reviews the thermal stability of ultra-fine grained (UFG) microstructure in selected magnesium and titanium-based materials prepared by severe plastic deformation (SPD). The focus is on the wide palette of experimental methods applicable for investigation of microstructural stability. These methods include scanning electron microscopy (SEM), electron backscatter diffraction (EBSD), microhardness measurement, positron annihilation spectroscopy (PAS), and electrical resistance measurement. Microstructural stability of UFG commercially pure (CP) Ti and Ti-6Al-7Nb alloy produced by equal-channel angular pressing (ECAP) is studied *ex situ* after annealing by SEM, by microhardness measurements, and *in situ* during heating, by high precision electrical resistance measurements. Both materials show stable UFG structure up to 440°C. Further annealing causes recovery and recrystallization of the microstructure. At 650°C, the microstructure is completely recrystallized. Magnesium alloy AZ31 is prepared by hot extrusion followed by ECAP. UFG microstructure recovers and continuously recrystallizes during annealing. The microstructure of UFG AZ31 alloy is stable up to 170°C and subsequent grain growth is analyzed. Special attention is paid to interpret the activation energy of the grain growth. The superplastic properties of UFG AZ31 alloy are investigated in the temperature range of 170–250°C.

Keywords: equal-channel angular pressing, magnesium alloys, titanium alloys, thermal stability, grain growth

1. Introduction

Lightweight metallic (especially titanium and magnesium) materials are extensively used in transport industry and in cutting-edge applications such as manufacturing of medical implants and devices. Ultra-fine grained (UFG) counterparts are still materials of the future, though the first commercial applications are emerging. In some applications, the employed materials are exposed to elevated temperatures either during service or during products manufacturing. Mechanical properties enhancement of materials prepared by severe plastic deformation (SPD) might be reduced due to recovery and recrystallization of the UFG microstructure at higher temperatures.

Magnesium alloys belong to materials with potential to replace aluminum or some other conventional structural materials in automotive, aircraft, and other industry branches. Magnesium and its alloys are light metals with relatively good mechanical properties which provide expanding potential in weight-critical applications. Interest in magnesium-based metals has recently been revived primarily due to their gradually decreasing costs and the effort of scientists, researchers, and engineers to cut down energy consumption and greenhouse gas emissions [1].

Utilization of titanium and titanium alloys for load-bearing orthopedic implants of big joints and for dental implants still increases [2–4]. Advantages of these materials include extreme corrosion resistance, sufficient biocompatibility, moderate elastic modulus, etc. [5]. A material with enhanced strength is required to reduce the size of the load-bearing orthopedic and dental implants. Vast majority of high-strength β-Ti alloys developed for an aircraft industry are not utilizable in biomedicine because of high content of toxic elements, such as vanadium [6, 7].

Ti-6Al-7Nb alloy was developed as a biocompatible alternative to the most used Ti-6Al-4V alloy. It belongs to α+β alloys which contain both α and β phases at ambient temperature. The β-transus temperature of this alloy is 1010°C [8]. UFG microstructure of the studied alloy has been already investigated in Ref. [9], and superior mechanical properties of UFG material were reported [10].

Promising possibility for strength and fatigue performance improvements is the manufacturing of materials with sub-micrometer or even nanoscale grain sizes using SPD techniques [11, 12]. These methods are very efficient in achieving significant grain refinement in polycrystalline materials. UFG materials have usually excellent mechanical properties including high strength and, if the UFG microstructure is sufficiently stable, a superplastic capability at elevated temperatures [11, 13]. Nowadays, the most attractive SPD techniques are equal-channel angular pressing (ECAP) [14] or combined process of extrusion followed by ECAP (EX-ECAP) [15], high-pressure torsion (HPT) [16], and accumulative roll-bonding [17]. In practice, ECAP or EX-ECAP processes are especially useful because of their simplicity in laboratory operation. Moreover, these techniques can produce relatively large billets for industrial applications [18]. There are several reports to date of the successful processing of magnesium and titanium materials using ECAP at elevated temperatures by employing different processing procedures [19–26].

The practical applications of the UFG AZ31 magnesium alloy are limited due to a low microstructure stability at elevated temperatures that complicates the processing of final products in industry. Thermal stability depends on many variables, such as stacking fault energy of the material, processing or volume fraction of grain boundaries, and their properties [27]. Microstructure stability at elevated temperature can be improved by various alloying elements or composite reinforcements. Microstructure stability of the AZ31 magnesium alloy after ECAP was studied by Kim [28] or Radi and Mahmudi [29], who investigated the AZ31 alloy reinforced by alumina nanoparticles. Both papers present calculations of grain growth activation energies which identified two or three temperature regimes with significantly different values of activation energy.

The main objective of this work is the investigation of microstructure stability during annealing of the UFG materials, in particular of the AZ31 magnesium alloy, commercially pure titanium (CP Ti) and Ti-6Al-7Nb alloy prepared by ECAP.

2. Materials and methods

As cast commercial AZ31 magnesium alloy (nominal composition of Mg-3%Al-1%Zn) was extruded at 350°C with an extrusion ratio of 22; subsequently, it was processed by four passes of ECAP. ECAP pressing was performed at 180°C with the velocity of 50 mm/min following route B_C, i.e. rotating the sample by 90° between the individual passes. The angle between two intersecting channels and the corner angle were $\Phi = 90°$ and $\Psi = 0°$, respectively. Both channels had a square cross section of 10 × 10 mm. The ECAP die was equipped with an ejector that allows pushing the sample out of the die immediately after pressing from the feed-in channel to the exit channel.

Flat squared specimens were cut from the middle part of the billets perpendicular to the pressing direction. Results of the microstructural observations and microhardness measurements on planes parallel to the pressing direction are very similar to those from the perpendicular plane [30] and were not addressed in this work.

CP Ti Grade 4 [31] was processed by ECAP through die with the round channel having the diameter of 15 mm. The channel angle was $\Phi = 105°$ and the corner angle $\Psi = 20°$. The temperature of the die during pressing was 300°C. The billets were pressed six times (six passes) following the route B_C at a constant ram speed of 60 mm/min. A detailed study of the ECAP processing of CP Ti can be found in Ref. [32]. Benchmark coarse grained material was prepared by annealing of the as-received material at 800°C for 2 h followed by slow cooling in furnace.

Ti-6Al-7Nb alloy was prepared by multi-step thermal sequence before processing by ECAP. The thermal treatment consisted of two subsequent annealing steps. The first annealing was at 985°C (a temperature just below β-transus) for 1 h and the second annealing at 780°C for 4 h. Each thermal treatment was followed by water quenching. The annealed material possesses a common "duplex" structure, which consists of 18 vol.% of primary α-phase [31]. Such

microstructural condition allowed the successful material processing by ECAP. The ECAP die with round channel with the diameter of 20 mm and angles of $\Phi = 120°$ and $\Psi = 0°$ was used for processing. The samples were pressed six times (six passes) at the temperature of 600°C. Subsequently, extrusion to 10 mm at 300°C was applied. Finally, the material was aged at 500°C for 1 h to achieve the maximum strength level. More details about material and its processing can be found in Ref. [33]. Benchmark coarse grained material underwent the same thermal treatment including the annealing steps simulating the thermal history during ECAP and extrusion.

The samples of CP Ti and Ti-6Al-7Nb alloys were heated up to the three temperatures specified by *in-situ* electrical resistance measurements (described in detail below) and subsequently water quenched.

Specimens of AZ31 magnesium alloy for thermal stability investigation were prepared by isochronal annealing for 1 hour at the temperatures ranging from 150 to 500°C followed by water quenching. Specimens of AZ31 magnesium alloy were mechanically grinded on watered abrasive papers and then polished with polishing diamond suspensions of grade 3, 1 and ¼ μm. Flat samples for Vickers microhardness measurements (load 100 g, 10 s) with minimum surface scratches were obtained by this method. Finally, the specimen's surface was polished by argon ions (Gatan PIPS™), which guaranteed successful electron backscatter diffraction (EBSD) measurements. CP Ti and Ti-6Al-7Nb alloy were prepared by mechanical grinding and polishing using watered abrasive papers followed by three-step vibratory polishing. The polished samples were prepared for microhardness (load 500 g, 10 s) and SEM measurement.

For *in-situ* measurement of electrical resistance evolution during heating, a precise self-made apparatus utilizing a common four-point method was employed. The electrical current and voltage were measured simultaneously. The samples were placed in a specially designed furnace which allows precise heating of the sample in a protective argon atmosphere. The relative error of such measurement is lower than 10^{-4}, and the experimental values are acquired with the frequency of 2 Hz [34]. The dynamics of microstructural changes can be assessed from these measurements. The electrical resistance was measured during heating with the constant rate of 5°C/min up to 700 and 800°C for CP Ti and Ti-6Al-7Nb alloy, respectively. UFG conditions of both materials were investigated along with their annealed coarse grained (non-deformed) counterparts. The samples for these measurements require special design maximizing their effective length.

Microhardness of AZ31 alloy and CP Ti was measured by LECOM-400-A microhardness tester. For Ti-6Al-7Nb alloy, a QNESS A10+ microhardness tester was employed with automatic indentation and evaluation using the QPix Control Program. FEI Quanta 200 FX scanning electron microscope equipped with EDAX EBSD camera and OIM software was utilized for EBSD and microstructure observations.

Flat specimens of AZ31 magnesium alloy for tensile tests were machined and cut from ECAPed billets parallel to extrusion direction. The continuous measurements of *m*-parameter were performed on six samples from a single ECAPed billet. The gauge length was 16 mm,

and the thickness and width were approximately 1 and 4 mm, respectively. Tensile tests were performed using a screw-driven Instron 5882 machine at 175, 200, and 250°C. Computer-operated machine allows arbitrary control of cross-bar movement.

Atomic force microscopy (AFM) observations were performed to study the deformation mechanism. The tensile samples were carefully polished on grinding papers and using diamond pastes (3, 1, and ¼ μm) before the tensile test. The samples after deformation were observed using Bruker Dimension Edge AFM.

3. Results

3.1. *In-situ* electrical resistance measurements of CP Ti and Ti-6Al-7Nb alloy

Temperature dependence of electrical resistance of CP Ti after ECAP and of the annealed coarse grained material is shown in **Figure 1(a)**. The relative resistance $R(T)/R_0$, where $R(T)$ is the resistance measured as the function of temperature T and R_0 is the resistance at room temperature, is plotted at the vertical axis. During heating up to 700°C, the resistance increases almost three times. Initially, the resistance increases linearly, whereas above 300°C, the evolution with temperature becomes concave. Small difference between annealed and ECAPed

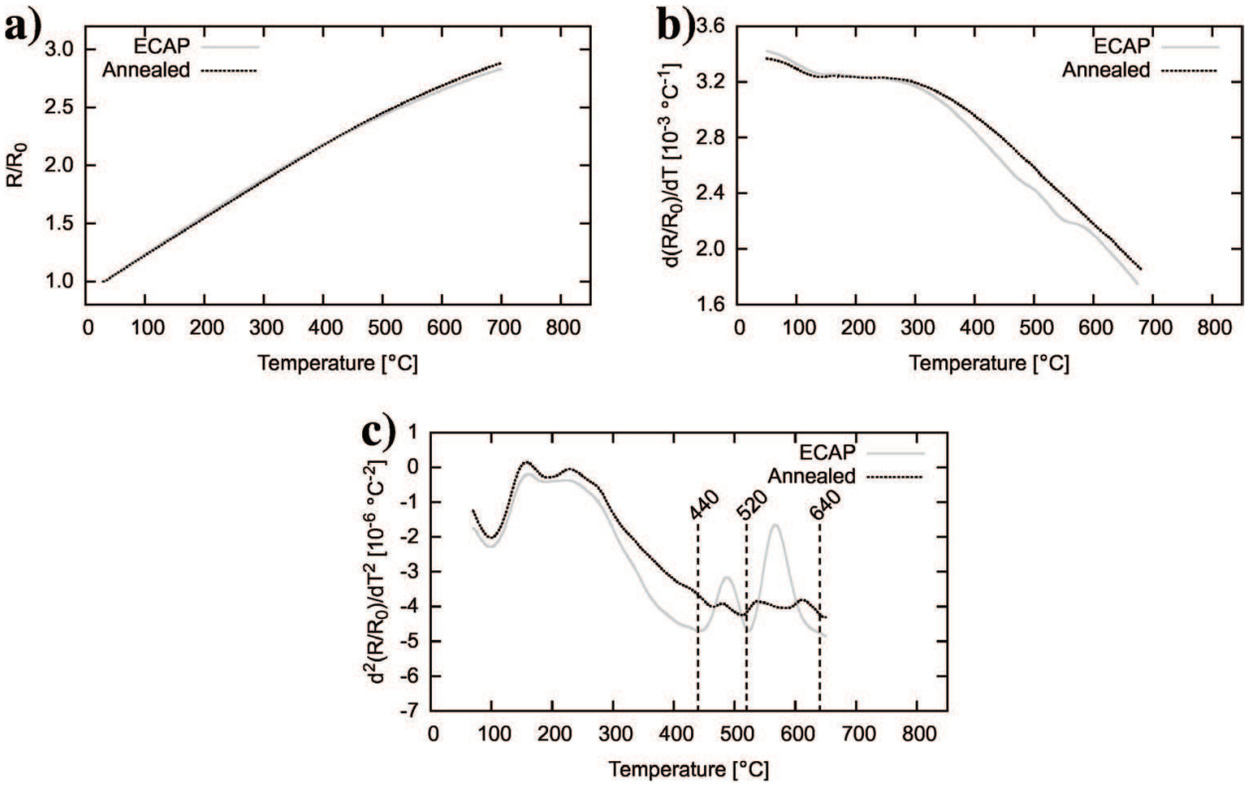

Figure 1. Relative resistance variations of CP Ti during heating (a) temperature dependence, (b) the first derivative of relative resistance, and (c) the second derivative of relative resistance (highlighted temperatures were chosen for SEM observation).

samples is observed. The first and the second derivatives of relative resistance with respect to temperature, computed numerically, are shown in **Figure 1(b)** and **1(c)**, respectively. In **Figure 1(b)**, both curves behave in a similar manner with two small deviations for ECAPed specimen at about 500 and 600°C. Those deviations appear as well observable peaks in the plot of the second derivative, which is plotted in **Figure 1(c)**. Assuming that these peaks correspond to undergoing microstructural changes, the temperatures of 440, 520, and 640°C were chosen for subsequent annealing and *ex-situ* observations of microstructure. All other peaks in the second derivative graph appear in both curves and therefore they do not represent differences caused by different initial microstructure.

Figure 2 shows the results of the resistance measurements of Ti-6Al-7Nb alloy that are presented in the similar way as for CP Ti. **Figure 2(a)** shows the temperature dependence of the relative resistance for the UFG Ti-6Al-7Nb alloy after ECAP and in the as-rolled condition. The relative resistance increases only by approximately 10%, in contrast to the CP Ti. The difference of the ECAP and as-rolled condition is therefore relatively more pronounced in **Figure 2(a)**. The overall course of both curves is concaved up to 650°C, and for higher temperatures, the electrical resistance even declines. **Figure 2(b)** shows the first derivative of electric resistance with respect to the temperature with two distinct peaks around 500 and 650°C for the ECAPed material. The differences between the two conditions are

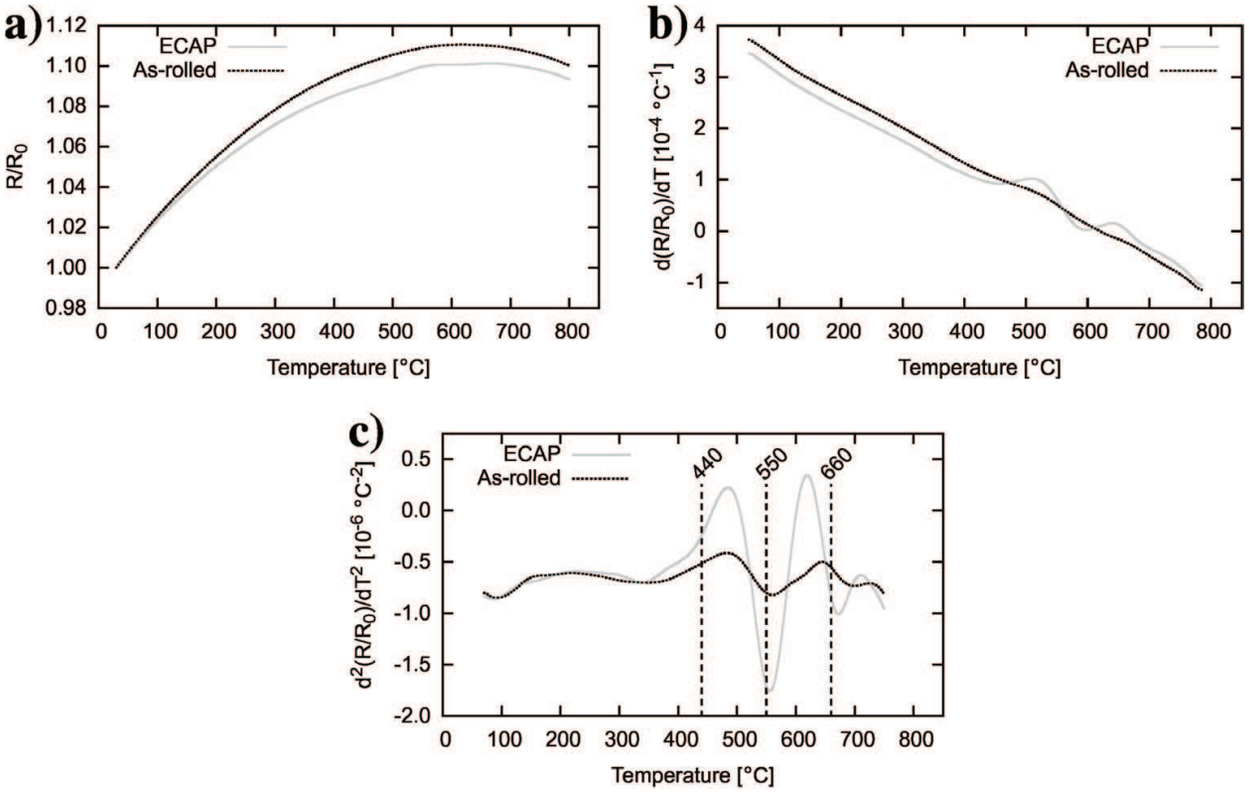

Figure 2. Relative resistance variations of Ti-6Al-7Nb alloy during heating (a) temperature dependence, (b) the first derivative of relative resistance, and (c) the second derivative of relative resistance (highlighted temperatures were chosen for SEM observation).

accentuated by plotting the second derivative of the electrical resistance as displayed in **Figure 2(c)**. The temperatures of 440, 550, and 660°C were selected for the microstructure observations using SEM.

3.2. Mechanical properties

The microhardness of the UFG materials after the SPD processing ($HV0.1_{AZ31}$ = 86, $HV0.5_{CPTi}$ = 274, and $HV0.5_{Ti67}$ = 369) is significantly higher than that of the annealed conditions ($HV0.1_{AZ31}$ = 58, $HV0.5_{CPTi}$ = 215, and $HV0.5_{Ti67}$ = 283) [31, 35, 36]. **Figure 3** depicts the microhardness dependence on the annealing temperature for each sample.

Microhardness values of the AZ31 alloy after annealing at 150 and 170°C do not differ significantly. However, the microhardness of the AZ31 declines abruptly in the temperature range of 170–230°C and then continues to decrease up to 500°C.

The values of microhardness of CP Ti remain nearly constant (HV0.5 ≈ 280) up to the aging temperature of 450°C and then decrease rapidly approaching values of annealed material at 700°C ($HV0.5_{annealed}$ = 215).

The annealed sample of Ti-6Al-7Nb exhibits the microhardness of $HV0.5_{annealed}$ = 283. The microhardness of ECAPed specimen increases up to (HV0.5 ≈ 370) and remains almost constant after heating to 440 and 550°C. Only heating to the highest temperature (660°C) results in a slight decrease of HV. However, the decrease of HV is much lower than in other investigated materials.

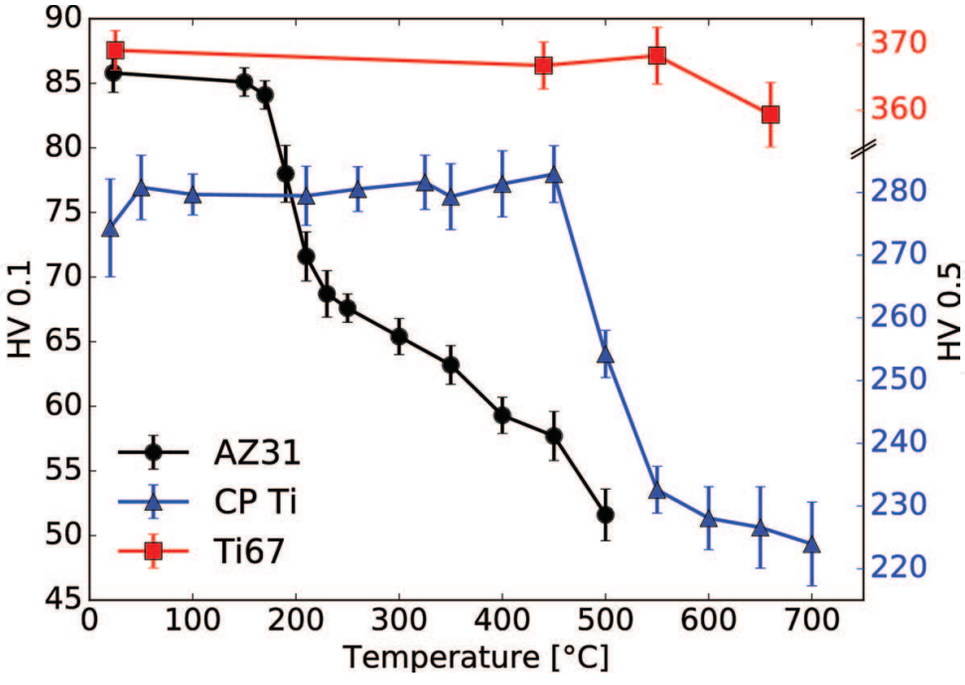

Figure 3. Microhardness of the studied materials subjected to SPD and heat treatment.

3.3. Microstructure

3.3.1. Microstructure changes and dislocation density evolution of UFG AZ31 alloy during heating

The microstructure of AZ31 magnesium alloy after extrusion (not shown here) is bimodal containing large grains elongated in the extrusion direction (≈10 μm) and smaller grains (≈1 μm) [36].

UFG microstructure of the specimen in the initial non-annealed condition (after extrusion and four passes of ECAP) is shown in **Figure 4(a)**. The microstructure is homogeneous comprising fine grains of the average size of 0.9 μm. The microstructure and average grain sizes of the samples after 1 h of isochronal annealing at 150 and 170**°C** (not shown here) are similar to the initial non-annealed specimen.

Inhomogeneous grain growth is observed at higher annealing temperatures (**Figure 4(b)–(f)**). Some grains start to grow at annealing temperatures of 190 and 210**°C** (the microstructure of the sample after annealing at 210**°C** is similar to that of 190**°C** and is not shown here). The fraction of coarse grains increases with increasing annealing temperature. At annealing temperature of 250**°C**, some areas with original fine grains are still observed. However, the small grains (≈1 μm) are continuously disappearing at higher annealing temperatures, and nearly no small grains are observed after annealing at 400**°C** (see **Figure 4(e)**). Please note that

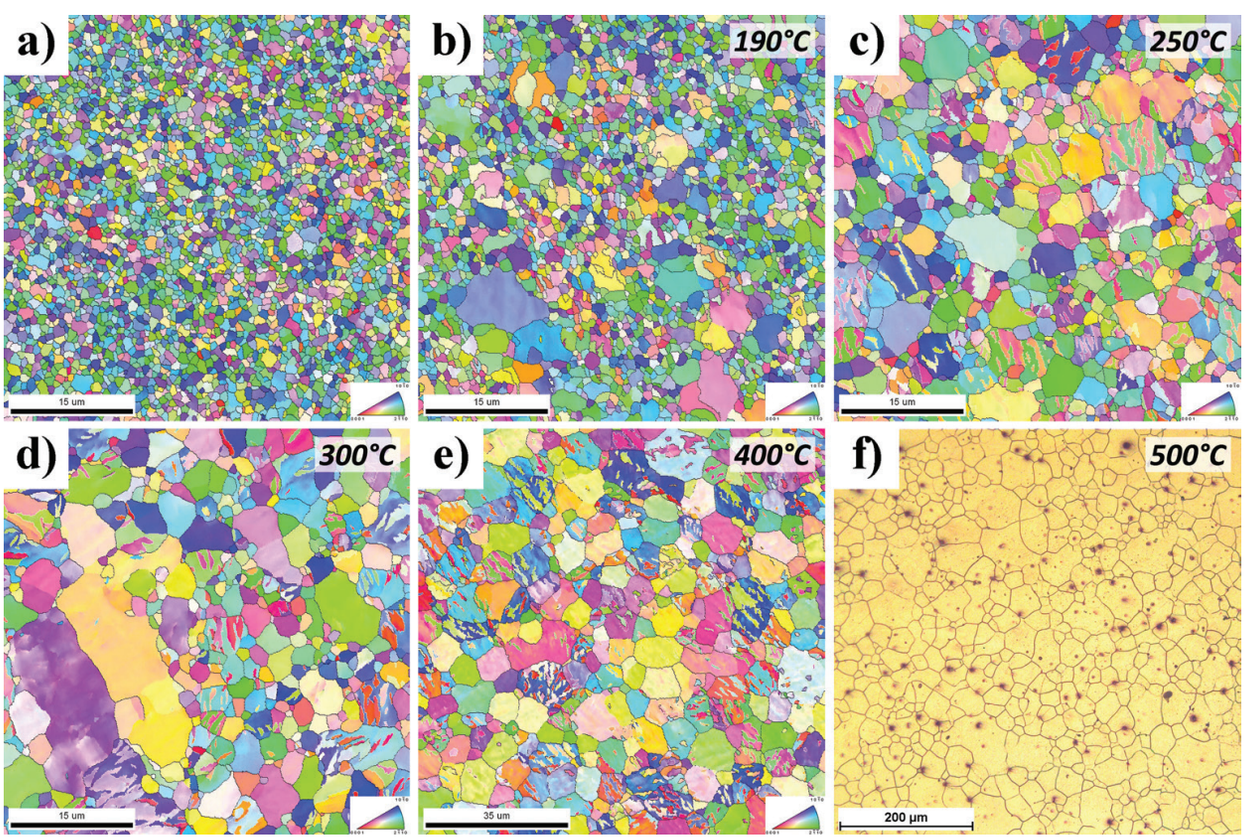

Figure 4. Microstructure of the AZ31 sample after extrusion and four passes of ECAP (a), and isochronally annealed at (b) 190°C, (c) 250°C, (d) 300°C, (e) 400°C, and (f) 500°C. Images (a)–(e) show results from EBSD measurements. The image (f) was taken using light microscope.

the magnification of the EBSD image in **Figure 4(e)** is two times smaller than the magnification of the previous EBSD images. Microstructure of the specimens annealed at 500**°C** was observed by light microscope (see **Figure 4(f)**).

The dependence of average grain sizes (number average) on annealing temperatures is plotted in **Figure 5(a)**. In specimens annealed at 250 and 300**°C**, the average values are calculated from the bimodal grain size distribution. The dependence of the average grain sizes and microhardness values on annealing temperature is summarized in **Table 1**.

Annealing twins observed after annealing at 250–400**°C** (see **Figure 4(c)–(e)**) were excluded from grain size calculations to achieve the true grain size values. All these twins were identified as the tensile twins with the misorientation angle of 86° [37].

The plastic shear deformation by extrusion and ECAP causes the accumulation of large plastic strain and the increase of density of structural defects. These defects are stable at room temperature, but they annihilate relatively easily during annealing.

The dependence of the mean dislocation density ρ_D measured by positron annihilation spectroscopy (PAS) for the samples subjected to annealing treatment at various temperatures is shown in **Figure 5(b)**. Dislocation density decreases with increasing annealing temperature and falls below the detection limit of PAS at annealing temperatures $T \geq 300$°C.

3.3.2. Microstructure changes of UFG CP Ti and Ti-6Al-7Nb alloy during heating

Microstructure changes in the UFG CP Ti and Ti-6Al-7Nb after ECAP occurring during linear heating were investigated *ex situ* by SEM. Samples in conditions corresponding to linear heating to the temperatures selected from *in-situ* electrical resistance measurements were observed (440, 520, and 640°C for CP Ti; 440, 550, and 660°C for Ti-6Al-7Nb alloy).

Figure 6 shows the microstructure of CP Ti, while in **Figure 6(a)**, the UFG microstructure of material after ECAP is displayed. White dots in the SEM micrograph are β-Ti particles formed due to contamination by iron, which is typical for CP Ti. High Fe content in these particles was proved by energy dispersive X-ray spectroscopy. The microstructure of the material is typical

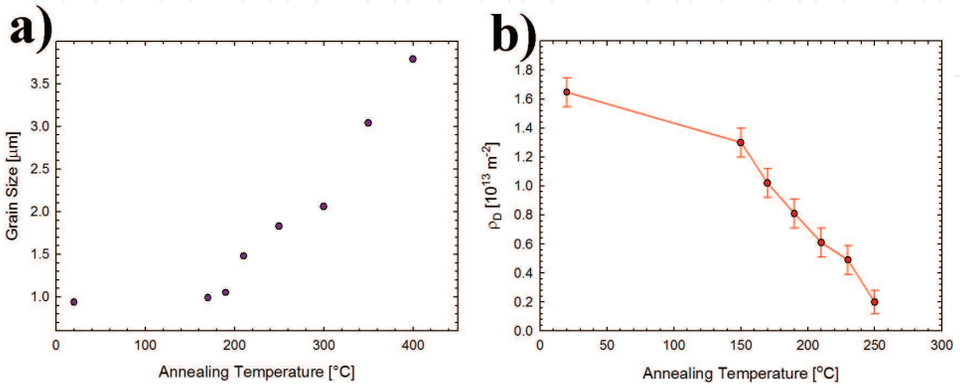

Figure 5. (a) Dependence of the average grain size (number average, excluding twins) of the AZ31 alloy on annealing temperature (up to 400°C). (b) Dependence of the dislocation density on annealing temperature after 1 h of isochronal annealing process.

Annealing temperature [°C]	–	170	190	210	250	300	350	400	450	500
Microhardness HV0.1	85.8	84.1	78.0	71.6	67.6	65.4	63.2	59.3	57.7	51.6
Average grain size *d* [mm]	0.94	0.99	1.05	1.48	1.83	2.06	3.04	3.79	10.09	24.53

Table 1. Microhardness values and average grain sizes at different annealing temperatures.

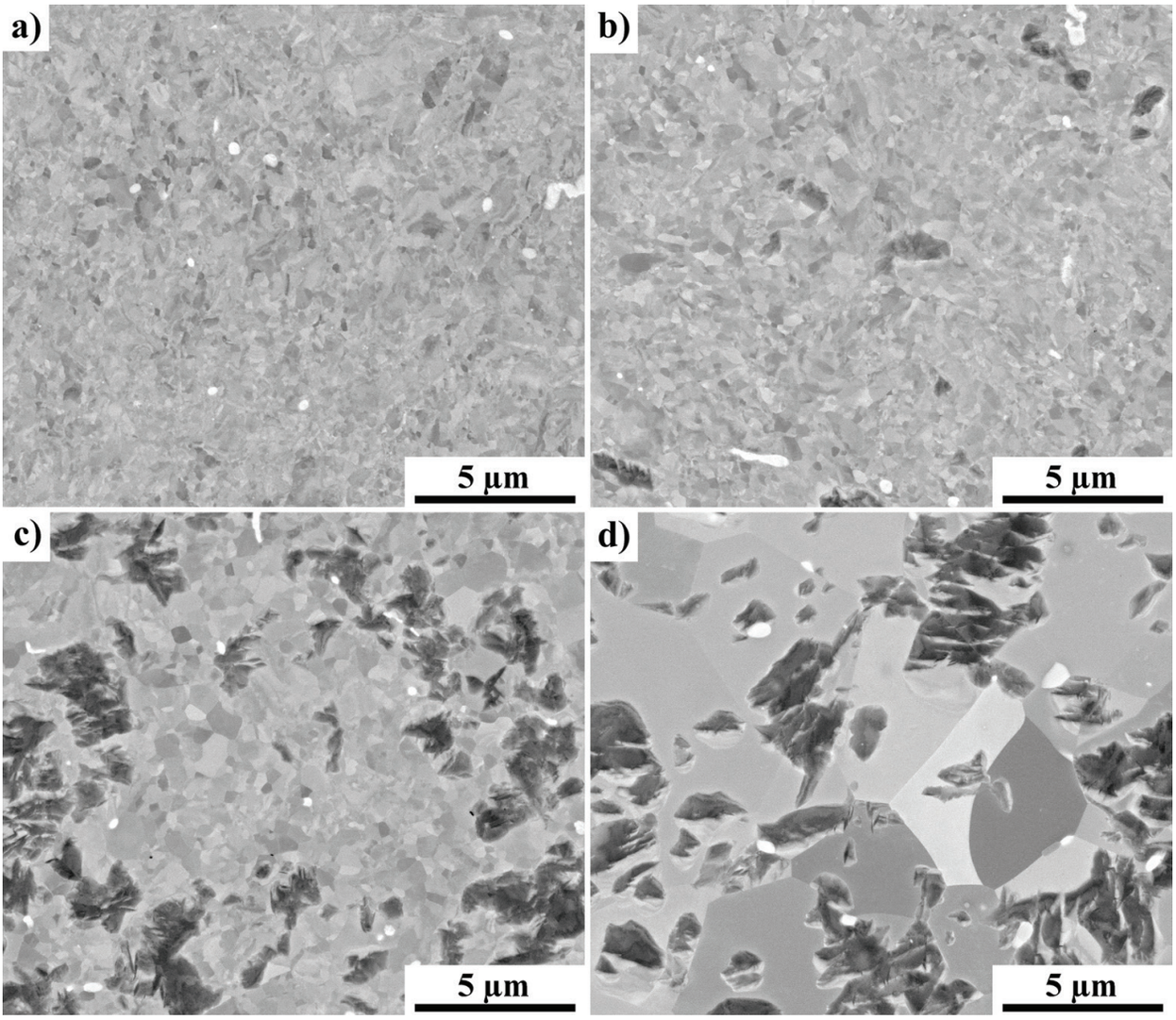

Figure 6. Microstructure evolution of ultra-fine grained CP Ti (a) as ECAPed, (b) heated to 440°C, (c) heated to 520°C, and (d) heated to 640°C.

heavily deformed containing grains with the average size around 1 μm [11, 38]. No significant differences of the microstructure were observed in the sample annealed up to 440°C (see **Figure 6(b)**). On the other hand, the microstructure of the sample annealed to 520°C differs considerably as can be seen in **Figure 6(c)**. The grains are much clearer, which suggests that

some recovery process, probably annihilation of dislocations, was undergoing during heating between 440 and 520°C. Grain size also slightly increased. The dark spots in the micrograph are probably artifacts caused by polishing. The microstructure of the specimen heated up to 640°C is shown in **Figure 6(d)**. Material is completely recrystallized with grains of the average size of approximately 5 μm.

Figure 7 shows the microstructure of UFG Ti-6Al-7Nb alloy after ECAP and subsequent heating. The material after ECAP, as shown in **Figure 7(a)**, has the typical duplex microstructure consisting of approximately 20% of heavily deformed primary α-phase and significantly fragmented α + β region, which contains slightly elongated β-phase particles appearing white in the micrograph due to chemical contrast. The microstructure of ECAPed specimen subsequently heated up to 440**°C** as shown in **Figure 7(b)**. There are no observable changes in the microstructure as compared to the ECAPed specimen. **Figure 7(c)** displays the material annealed up to 550**°C**. Detailed inspection of the micrograph reveals small fraction of tiny grains in α + β region with very clear contrast, suggesting that these are newly formed dislo-

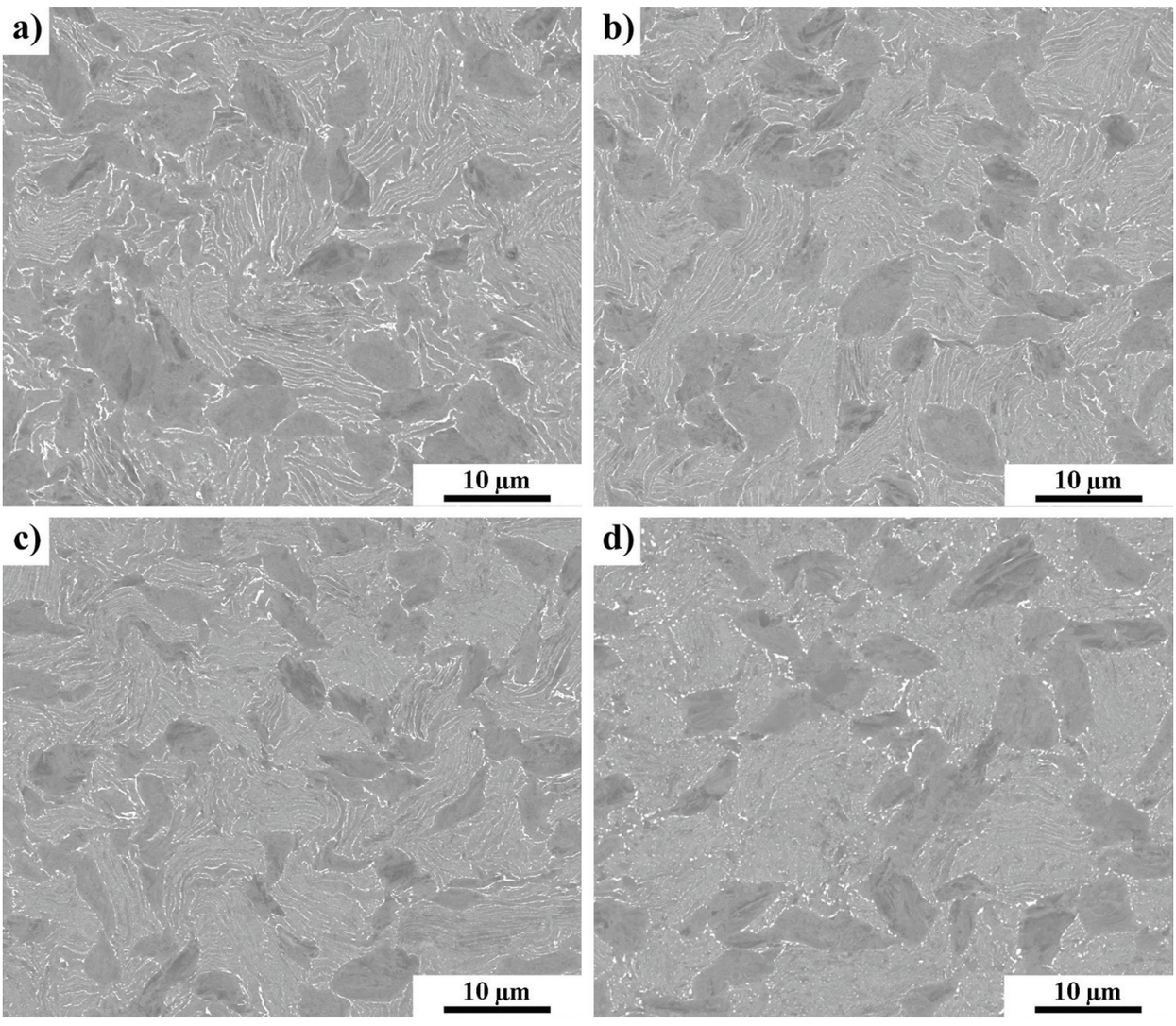

Figure 7. Microstructure evolution of UFG Ti-6Al-7Nb alloy (a) as ECAPed, (b) heated to 440°C, (c) heated to 550°C, and (d) heated to 660°C.

cation-free grains. Also β-phase particles are slightly globularized. Finally, in **Figure 7(d)**, the microstructure of the specimen annealed up to 660°C is shown. The microstructure is partly recrystallized with grains >1 μm in the originally heavily fragmented α + β region. White β-phase particles are significantly bigger and more globular.

3.4. Superplastic behavior of AZ31

3.4.1. Methodology of superplastic behavior determination

Two types of tests for strain-rate sensitivity determination were performed. Firstly, standard strain-rate changes tests were carried out to determine the *m*-parameter for a wide range of strain rates at selected temperature. True strain rate was increased in a step-wise manner from 5×10^{-5} to 10^{-2} s^{-1}. Maximum stress after approximately 2% deformation at each strain rate was recorded for the calculation of *m*-parameter.

Secondly, a special strain rate control test was undertaken. For the determination of the strain rate sensitivity at strain rate of $\dot{\varepsilon}_1 \approx 10^{-4}\,s^{-1}$, two different true strain rates were selected: $\dot{\varepsilon}_1 = 0.9 \times 10^{-4}\,s^{-1}$ and $\dot{\varepsilon}_2 = 1.2 \times 10^{-4}\,s^{-1}$. The actual true strain rate was changed every 120 s (i.e. after $\varepsilon \approx 1.2\%$) during the experiment. Note that the overall cross-bar speed exponentially increased to maintain the selected two true strain rates. Therefore, the overall true strain is proportional to the time ($\varepsilon = 100\% \sim t = 3h$). The methodology of continuous measurement of *m*-parameter during the tensile test is described in detail in our recently published paper [39].

Due to the strain rate sensitivity of the material and alternating strain, the resulting flow curve (thin curve in **Figure 8** for sample deformed at 200°C) has a saw-like character.

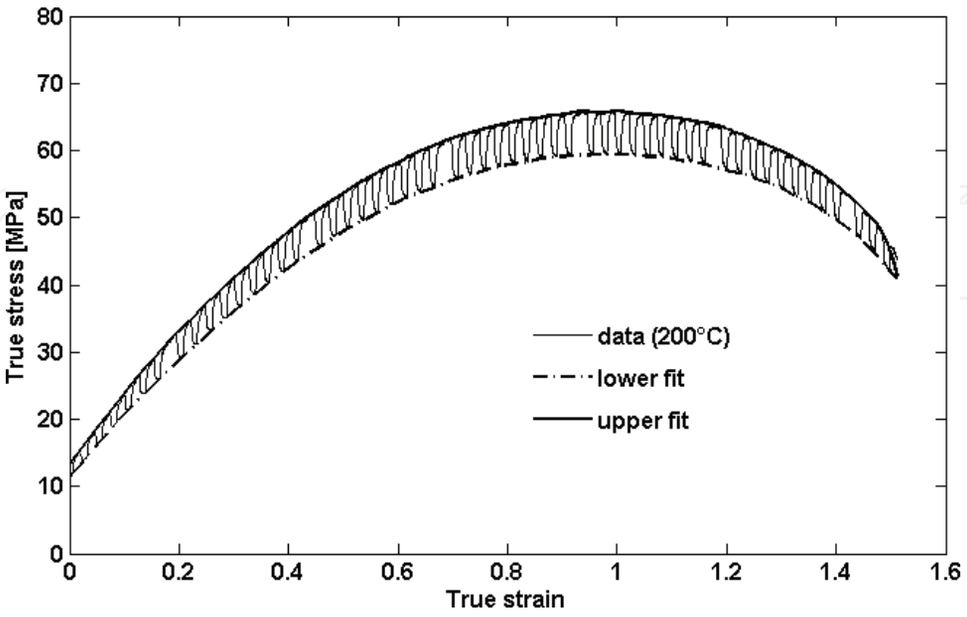

Figure 8. Measured flow curve for alternating strain rates (thin curve) and flow curves interpolated through local maxima and minima (thick smooth curves) for sample deformed at 200°C.

Local maxima of the alternating flow-curve were joined by a smooth curve regarded to as the "upper fit" which represents the approximate flow-curve at the higher strain rate $\sigma_2(\varepsilon)$, whereas the interpolation of local minima, the "lower fit", estimates the flow-curve at the lower strain rate $\sigma_1(\varepsilon)$. As a result, the continuous evolution of m-parameter with strain can be calculated as:

$$m(\varepsilon) = \frac{ln(\sigma_2(\varepsilon)) - ln(\sigma_1(\varepsilon))}{ln(\dot{\varepsilon}_2) - ln(\dot{\varepsilon}_1)}. \quad (1)$$

Note that the denominator in Eq. (1) depends only on the selected true strain rates and is constant.

3.4.2. Results: superplastic behavior of UFG AZ31 alloy

The evolution of m-parameter with strain rate is depicted in **Figure 9** for testing temperatures of 175, 200, and 250**°C**. Material exhibits the superplastic behavior ($m > 0.5$) at all studied temperatures and strain rates up to 10^{-4} s^{-1}. At intermediate temperatures of 175 and 200**°C**, the range of $m > 0.5$ extends to strain rates of 5×10^{-4} s^{-1}. For strain rates higher than 10^{-3} s^{-1}, the material is not superplastic ($m < 0.3$) at all studied temperatures.

Based on these results, the strain rate of 10^{-4} s^{-1} and temperatures of 175, 200, and 250**°C** were selected for further testing employing alternating strain rate, as described in the previous section. Two samples per condition were tested. **Figure 10** shows the measured true stress-true strain flow curves. Both measured flow curves for each condition are shown to assess the reproducibility of the experiment. All flow curves exhibit significant strain hardening,

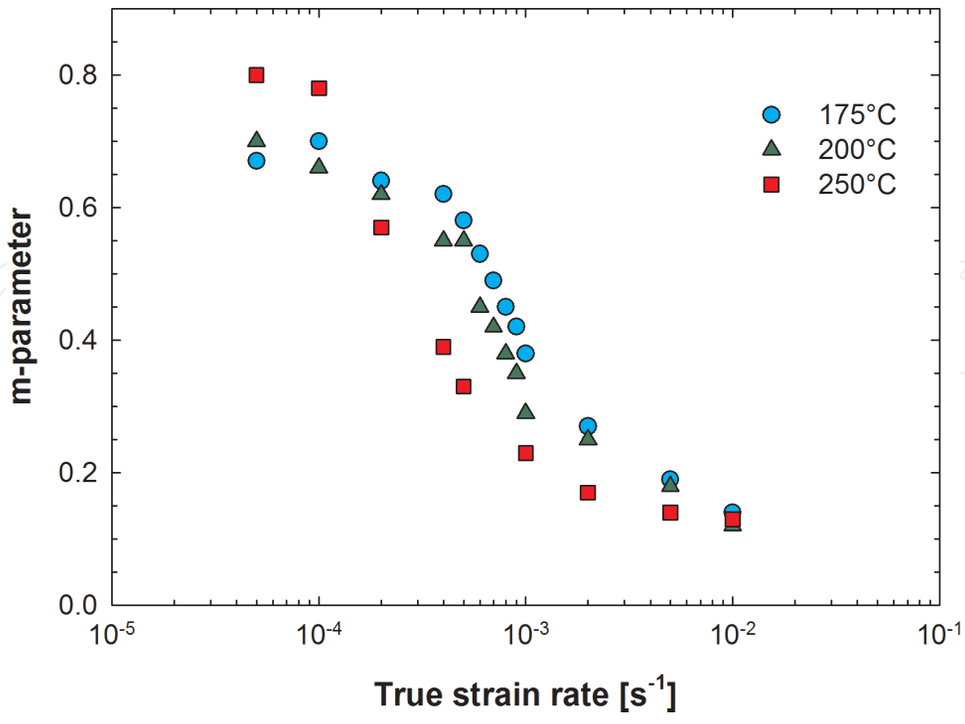

Figure 9. Measured m-parameter at deformation temperatures 175, 200, and 250°C.

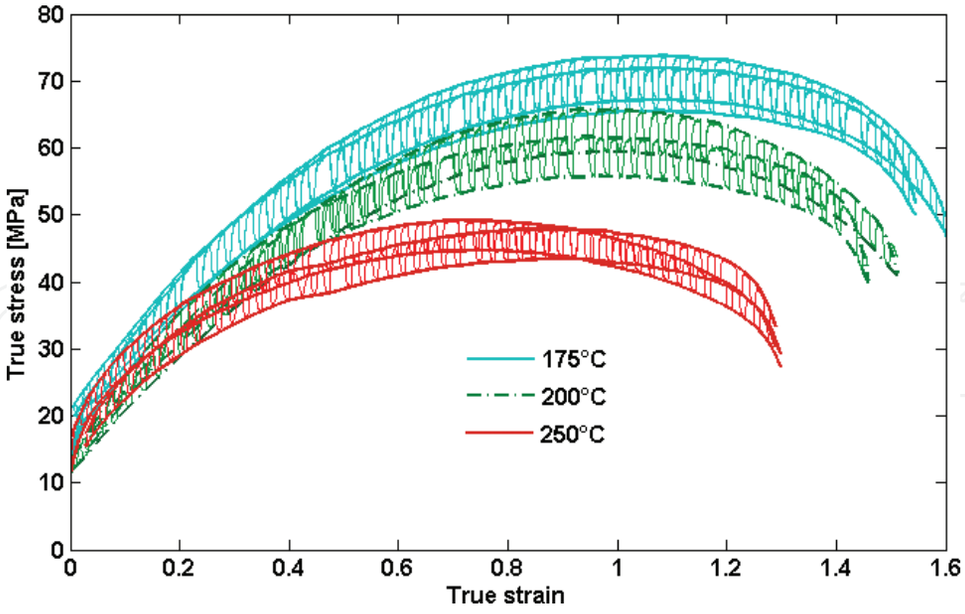

Figure 10. True stress-true strain curves for six tested samples. Measured flow curve for alternating strain rates (thin curve) and flow curves interpolated through local maxima and minima (thick smooth curves).

which is followed by moderate softening. In the final stage of deformation, observed softening is much more pronounced and the strain rate sensitivity decreases, which suggests that the specimen undergoes the strain localization. As expected, the highest stress is achieved at the lowest testing temperature of 175°C. However, the samples tested at 175°C exhibited surprisingly the highest elongation to fracture ≈ 380% (true strain ε ≈ 157%). The flow curves for 200°C, and especially 250°C, reached the lower maximum true stress, which was also achieved at lower true strain. Shorter range of strain hardening seems to be responsible for lower achieved total elongation, especially in samples deformed at 250°C.

The *m*-parameter evolution $m(\varepsilon)$ calculated from Eq. (1) for all investigated samples is depicted in **Figure 11** [39]. In the beginning of test, the *m*-parameter reaches 0.5 and then decreases with increasing true strain to values slightly above 0.3. The *m*-parameter for samples deformed at 250°C is lower in the initial stage of the deformation, while the *m*-parameter for samples deformed at 200°C is the highest at the true strain $\varepsilon > 1$. Final sharp decrease of *m*-parameter is associated with necking.

Achieved elongation and *m*-parameter values suggest superplastic deformation mediated by grain boundary sliding. If a sample with polished smooth surface is deformed in superplastic regime by grain boundary sliding, individual grains can be observed on surface using atomic force microscopy (AFM) [40–42]. Tensile sample deformed at 150°C with the constant strain rate of 10^{-4} s^{-1} which achieved elongation of 315% was used for AFM measurement. **Figure 12(a)** shows the deformed region far from the neck. This region was deformed superplastically, and individual grains with the size of ~1 μm can be observed. On the other hand, **Figure 12(b)** shows the region close to the tip of the neck, where the failure occurred. Slip bands appear as typical steps and grain structure cannot be resolved.

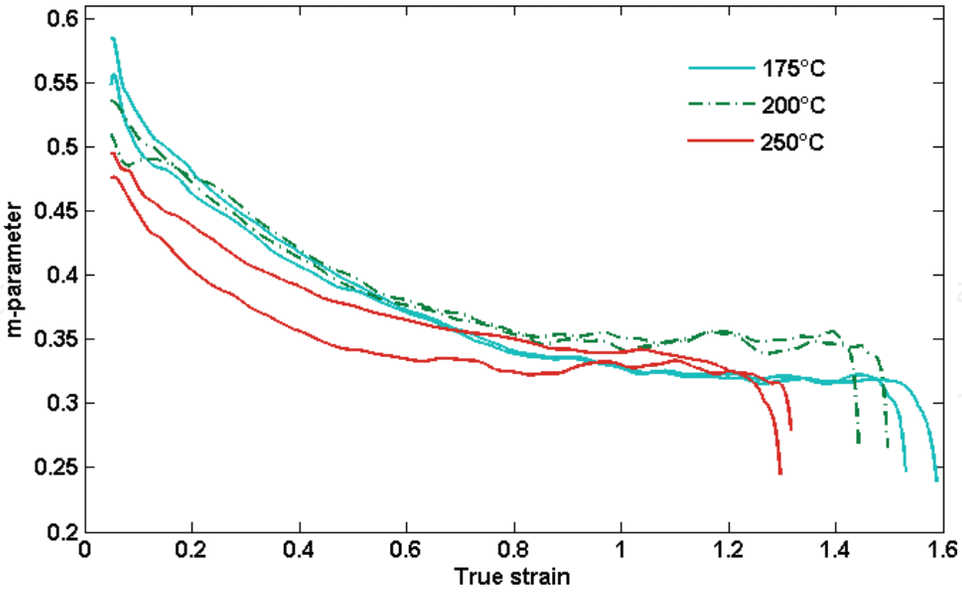

Figure 11. Evolution of *m*-parameter determined from interpolated flow curves for samples deformed at 175, 200, and 250°C.

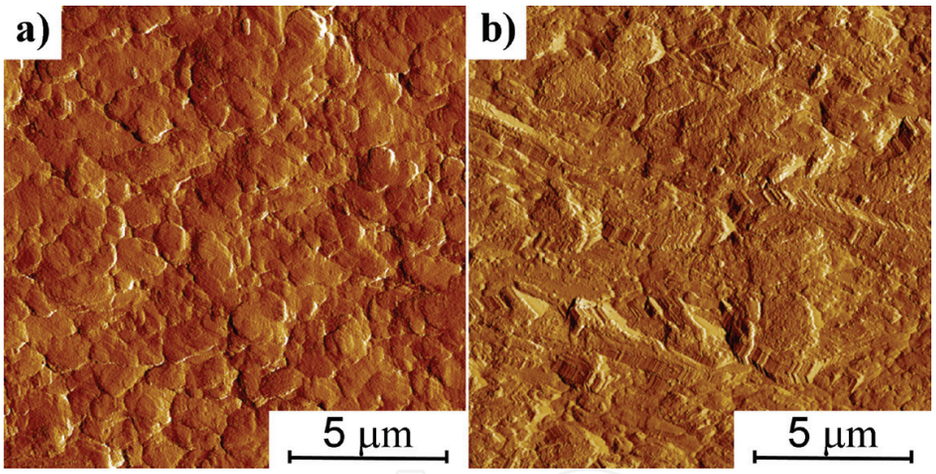

Figure 12. AFM image of a surface after deformation: (a) deformed region far from the neck, (b) deformed region in the neck.

4. Discussion

4.1. AZ31 magnesium alloy

4.1.1. Correlation between mechanical properties, dislocation density, and microstructure

Microhardness measurements (cf. **Figure 3**) indicate that UFG microstructure of AZ31 magnesium alloy is stable up to 170°C. After annealing at temperatures higher than 190°C, a sharp drop of microhardness occurred. A detailed inspection of the temperature dependence of the microhardness (cf. **Figure 3**) indicates a two-step character of the microhardness decline. In

the lower annealing temperature range (170–210°C), the decline is significantly sharper, while for higher annealing temperatures (T > 210°C), the slope of the curve is much lower.

This two-step character of the curve suggests a change of the mechanism controlling mechanical properties. The strength and microhardness of severely deformed UFG materials are affected mainly by the dislocation density [43] and the grain size according to the Hall-Petch relation [44, 45]. Therefore, the grain coarsening and the dislocation annihilation during annealing are expected to control the material strength and microhardness.

Figure 5(a) shows the grain sizes evolution, which could be correlated with dislocation density evolution with annealing temperature shown in **Figure 5(b)**. In the low temperature region of the microhardness drop (T ≈ 170–210°C), the grain growth is relatively negligible (see **Table 1**), whereas the dislocation density gradually declines indicating a recovery of dislocation structure. Most probably rearrangement and mutual annihilation of dislocations with opposite signs take place during annealing in this lower temperature range (T < 210°C). As seen in **Figure 4(b)** and **(c)**, the fine grain structure becomes unstable and significant grain growth is observed at temperatures T > 210°C. In this temperature range, the dislocation density is very low, falling below the detection limit of PAS ($\rho_D \approx 10^{12}$ m^{-2}) at T ≈ 300°C [36].

From microstructure observation (using EBSD) and lattice defect density determination (using PAS), one can conclude that in the lower annealing temperature region (T ≈ 180–210°C), it is mostly the annihilation of dislocations which causes the drop of microhardness. At higher annealing temperatures (T > 210°C), probably the grain growth influences significantly the hardness of AZ31 magnesium alloy.

4.1.2. Grain growth analysis

The determination of grain size in UFG material allows analyzing the mechanisms of grain growth during annealing. Two microstructural aspects may be determined:

(a) The activation energy of grain growth

The grain growth mechanism during static annealing can be assessed from calculated activation energy of grain growth. For this analysis, we can use the general equation of the grain growth

$$d^n - d_0^n = kt, \tag{2}$$

where d is the grain size after given annealing time, d_0 is the initial grain size, n is the grain growth exponent, t is the annealing time, and k is a temperature-dependent constant which can be described by Arrhenius equation:

$$k = k_0 \exp\left(-\frac{Q}{RT}\right), \tag{3}$$

where k_0 is a constant, Q is the activation energy of grain growth, R is the universal gas constant, and T is the thermodynamic temperature.

The value of the stress exponent n is of significant importance. In the ideal case (defect-free infinite crystal), the grain growth exponent n should be equal to 2. However, higher values of n are very often found, which can be attributed to various factors affecting grain growth kinetics, such as the effect of free surface, texture, impurity-drag, dislocation substructure, and microstructure heterogeneities [46]. Several studies [47–49] reported a value of n in a range from 2 to 8 for various magnesium alloys and magnesium-based composites. Higher values of n ($n \geq 5$) were observed mainly in UFG magnesium materials produced by mechanical alloying [48, 49]. The value of grain growth exponent n observed in ultra-fine grained magnesium alloy AZ31 produced by various techniques of severe plastic deformation ranges between 2 and 4 [47, 50, 51]. The AZ31 alloy processed similarly as the investigated material (ECAP without previous hot extrusion, where the average grain size after 4 passes was equal to 2.5 μm) was studied by Kim [28] and Kim and Kim [47]. The grain growth exponent n used in their calculations was equal to 2. We use the same value of n, which will allow us to make a direct comparison with the results of Kim and Kim [47].

Considering isothermal annealing and substituting Eq. (3) into Eq. (2), one can determine the activation energy Q as the slope of the dependence of $ln(d^2 - d_0^2)$ on T^{-1} which is shown in **Figure 13** for the investigated AZ31 alloy. Three temperature ranges with different Q values can be distinguished. The calculated values of activation energy of grain growth are 115, 33,

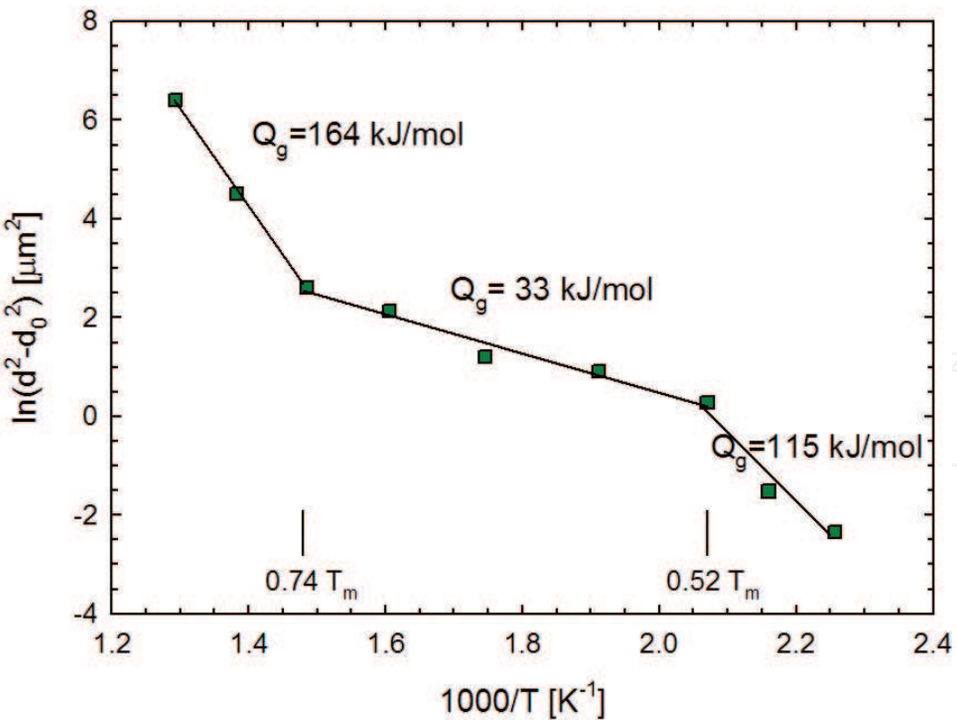

Figure 13. Plot of $ln(d^2 - d_0^2)$ vs. T^{-1} for the estimation of the activation energy of grain growth of the EX-ECAP magnesium alloy AZ31.

and 164 kJ/mol in the temperature ranges 170–210, 210–400, and 400–500°C (443–483, 483–573, and 573–673 K), respectively. These three temperature ranges with different Q values were observed in other fine-grained AZ31 alloys in various conditions, and the respective temperature ranges are very similar with our temperature ranges [39, 47].

In the low temperature range (T< 483 K, <210°C), the activation energy is relatively high—higher than the activation energy of grain boundary diffusion in pure magnesium (92 kJ/mol [52]), but, on the other hand, much lower than the activation energy of lattice self-diffusion (135 kJ/mol [53]). Considering a well-known fact that the activation energy of alloys should be higher than the activation energy of pure metals, the diffusion mechanism can be attributed to the grain boundary diffusion, which might be further affected by dislocations. In this temperature range, the dislocation density within the grains decreases with increasing temperature, but it remains relatively high.

In the high temperature range (T > 673 K, > 400°C), the activation energy Q is equal to 164 kJ/mol, which is higher than lattice self-diffusion in pure magnesium (135 kJ/mol [53]). The lattice self-diffusion is activated, and the grain growth leads eventually to fully-recrystallized structure.

In the intermediate temperature range, the value of Q is abnormally low. Similarly, low value of Q was reported by Wang et al. [54] in the ECAPed Al-Mg alloy annealed at the temperatures $T \leq 275$°C. The authors attribute the extremely low value of Q to the non-recrystallized microstructure with a certain fraction of non-equilibrium grain boundaries. This conclusion is consistent with the concept of reduced activation energy of grain boundary diffusion in UFG materials produced by SPD caused by the ability of the non-equilibrium grain boundaries to provide enhanced atomic mobility [55, 56]. The AZ31 alloy after extrusion and 1 pass of ECAP contains a significant number of non-equilibrium grain boundaries. However, the fraction of non-equilibrium grain boundaries decreases with increasing number of ECAP passes so that nearly no such grain boundaries are observed in more deformed AZ31 alloy [57].

It is shown in Kim and Kim [47] and supported by our results that the low fitted value of apparent activation energy in the intermediate temperature range 210–400°C cannot be substantiated. It is argued in [47] that the mechanism of diffusion that is the driving force for grain growth is continuously changing due to recovery processes and therefore the Arrhenius equation (Eq. (1)) is not valid. Detail computation provided in Ref. [58] shows that if true activation energy of the process responsible for the grain growth continuously rises from the activation energy of grain boundary diffusion (115 kJ/mol) to the activation energy of lattice self-diffusion (164 kJ/mol), then the (wrong) fitting by a single Arrhenius equation indeed results in very low (and physically meaningless) estimate of apparent activation energy (33 kJ/mol). Based on a simple model assuming continuous increase of activation energy [58], it can be concluded that the dominant diffusion process is the grain boundary diffusion up to 210°C, while the lattice self-diffusion is dominant from 400°C. In the intermediate region, the effect of grain boundary diffusion decreases due to undergoing grain growth.

(b) Hall-Petch relation

EBSD analysis allows us to determine the validity of the Hall-Petch relation for isochronally annealed UFG AZ31 alloy in the temperature range up to 400°C. For this analysis, the Hall-Petch relation yields

$$HV = H_0 + K_H d^{-\frac{1}{2}}, \tag{4}$$

where HV is the measured value of microhardness and H_0 and K_H are material constants.

The dependence of HV on d determined from **Figures 3** and **5**, respectively, is plotted in **Figure 14**.

The constants H_0 and K_H may be calculated from the parameters of a linear fit depicted also in **Figure 14**. The best fit was applied only to data corresponding to higher annealing temperatures (from 250 to 500°C) since in this temperature range, only the grain size affects the material hardness as the dislocation density is low (cf. **Figure 5(b)**). At low temperatures, both the reduced grain and the high dislocation density contribute to strengthening as one may assess from **Figures 5(a)** and **(b)**, and the linear fit of microhardness data fails. Data for low annealing temperatures (i.e. high dislocation density conditions) lie clearly above the Hall-Petch fit (the difference is marked by the arrow in **Figure 14**).

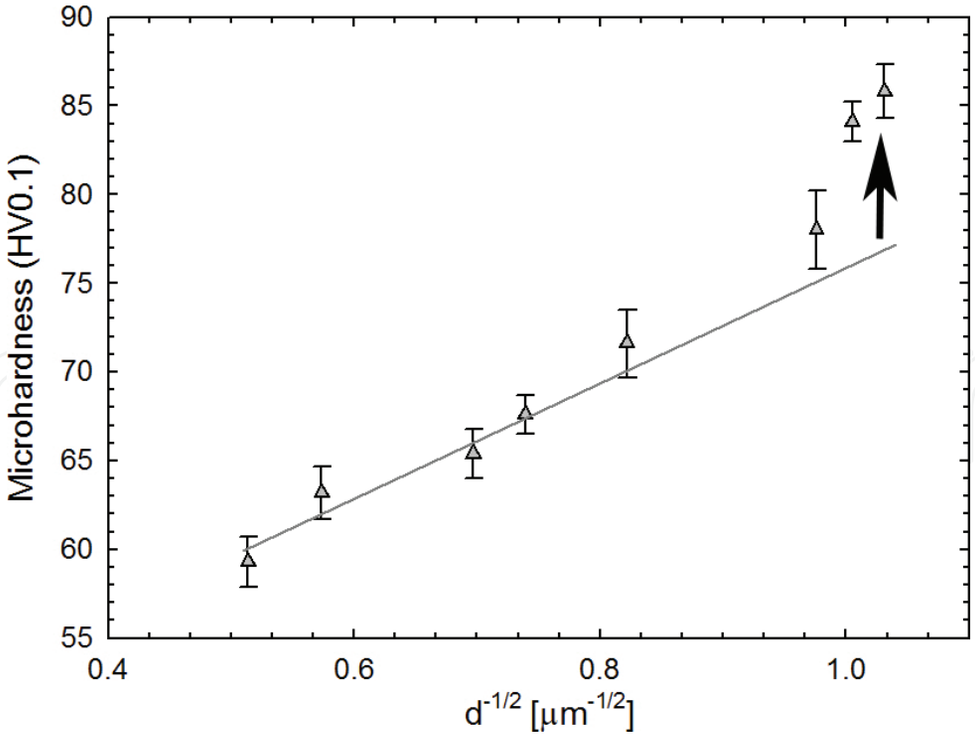

Figure 14. The Hall-Petch relationship for the isochronally annealed EX-ECAP AZ31 alloy based on HV0.1 microhardness data.

The calculated material constants from the high temperature fit of *microhardness* versus $d^{1/2}$ are: $H_0 = 47 \pm 2$ and $K_H = 27 \pm 3$ μm$^{1/2}$. These values are partly comparable to those reported on Al alloys prepared by ECAP ($H_0 = 35–47$ and $K_H = 35–50$ μm$^{1/2}$) [59], but different from those reported on the UFG AZ31 alloy reported by Kim and Kim [47] ($H_0 = 38$, $K_H = 42$). It might be argued that the constants in Ref. [47] were calculated from the linear fit of the whole temperature range because the changes of dislocation densities were not taken into account. It results in underestimating and overestimating of H_0 and K_H constants, respectively, in comparison with our calculated values. Our value of the constant H_0 is closer to the microhardness value of the AZ31 in annealed condition (HV0.1 = 58 ± 3, see Ref. [60]) than the value of H_0 calculated by Kim and Kim [47].

4.1.3. Superplastic behavior

AZ31 magnesium alloy processed by ECAP exhibited a superplastic behavior at comparatively low temperatures of 150–250°C at low strain rates up to 5×10^{-4} s^{-1} according to *m*-parameter evaluation. This is consistent with previous studies investigating ultra-fine grained AZ31 alloy [61–64]. However, the elongation of studied samples did not reach 400%. This may be partly attributed to the size of used specimens. In this study, we used samples with relatively long gauge length of 16 mm. In this case, final strain localization—necking—is responsible for negligible elongation. On the other hand, if small samples are used (the gauge length ~ 1 mm), necking before failure provides significant additional elongation.

At elevated temperatures, the diffusion processes are generally enhanced and contribute to the superplastic behavior. However, we found that *m*-parameter does not increase with the temperature and achieved elongation even slightly decreases. This unusual behavior can be attributed to recovery and recrystallization processes at elevated temperatures. Diffusion of atoms, which facilitates superplastic behavior, is enhanced by fast diffusion paths like pipe diffusion along dislocations or grain boundaries, which was found as the dominant diffusion processes in severely deformed UFG microstructure [30, 58, 65]. Note also that the activation energy of grain boundary diffusion in pure Mg (92 kJ/mol [52]) is much lower than the activation energy of self-diffusion (135 kJ/mol [53]). The decrease of *m*-parameter and the total elongation for 250°C is therefore probably caused by disappearing of fast diffusion paths due to recovery and grain growth. Limited work hardening at 250°C is also attributed to recovery processes, which occur even during static annealing at 250°C [36, 66], and the grain growth might be even faster under dynamic conditions [67]. On the other hand, during annealing at 175 and 200°C, limited decrease of dislocation density was observed [36]. The *m*-parameter during deformation at 200°C remains higher than at 175°C (possibly due to simple temperature effect on diffusion).

4.2. CP Ti and Ti-6Al-7Nb alloy

4.2.1. Resistance evolution

The electrical resistance of CP Ti showed in **Figure 1** increased approximately three times during heating up to 700°C as compared to the room temperature value. In fact, the resistivity increase with increasing temperature in CP Ti depends upon the amount of impurities (mainly oxygen).

The achieved results for CP Ti Grade 4 are in good agreement with other authors [68]. Much smaller increase of resistance (by only 10%) in Ti-6Al-7Nb alloy as compared to CP Ti confirms the well-known fact that the structural/compositional component of resistance in alloyed systems is higher by one order of magnitude than the temperature-dependent component [69]. The decrease of the resistance in Ti-6Al-7Nb alloy above 700°C is caused by increasing equilibrium amount of β-phase with increasing temperature. Note that the Ti-6Al-4V alloy containing approximately 15% of β-phase particles at 750°C and 20% of β-phase particles at 800°C exhibited the similar resistance decrease [70]. The most important result is the obvious difference in resistance evolution between UFG materials and their coarse grained counterparts. This difference is more apparent in the Ti-6Al-7Nb alloy and is probably caused by more pronounced structural effect on overall resistance than in CP Ti. In the CP Ti, the difference in resistance evolution is almost certainly caused by recovery and/or recrystallization as no structure changes occur in the investigated temperature range. We assume, however, that recrystallization and/or recovery is also responsible for the differences in resistivity evolution in Ti-6Al-7Nb. However, in this alloy, other effects including changes in β-phase particles morphology, reduced amount of phase interfaces, and also increasing equilibrium amount of β-phase at elevated temperatures are expected to affect the overall resistance.

4.2.2. Correlation between mechanical properties and microstructure

The CP Ti processed by ECAP exhibits nearly constant value of microhardness after annealing at temperatures lower than 450–500**°C** (**Figure 3**). In this temperature range, the recovery of the material starts and the microhardness declines. The microhardness data are consistent with the electrical resistance measurements. Observations by scanning electron microscopy (**Figure 6**) revealed that material recovery/recrystallization is responsible for the first bump in the first derivative of resistance and the decrease of materials microhardness.

Similarly to the CP Ti, the microhardness of the UFG Ti-6Al-7Nb alloy remains constant during heating up to 440 and 550**°C**. Note that both annealed and UFG samples of Ti-6Al-7Nb alloy were heat treated at 500**°C** for 1 hour, which is considered as a strength increasing heat treatment [71, 72]. Heating of UFG samples up to 440 and 550**°C** does not affect the microhardness, despite an obvious response of the electrical resistivity, which can be probably attributed to the recovery process. It is therefore assumed that an initial stage of the recovery process has only a negligible effect on the microhardness in Ti-6Al-7Nb alloy. The annealing of the sample up to 660**°C** leads to a slight decrease of the microhardness. The effect of heating on microhardness is much lower in Ti-6Al-7Nb alloy than in CP Ti due to solid solution strengthening and, even more importantly, due to strengthening by phase interfaces.

SEM observations of CP Ti did not reveal any microstructural changes after heating up to 440**°C**. It is consistent with the electrical resistance evolution and microhardness measurements and also with the results of other authors [73]. Thermally activated processes in CP Ti during annealing up to 440**°C** were not observed. Further annealing to 520**°C** caused significant recovery and possibly even the initial stage of recrystallization/grain growth. These processes are responsible for significant decrease of microhardness. Annealing up to 640**°C** caused complete recovery and recrystallization. Such processes were apparently detected by

in-situ measurement of electrical resistance. The results proved that high sensitivity *in-situ* measurement of electrical resistance is capable of detecting recovery and/or recrystallization processes in temperature regions that are decisive for microstructure stability of UFG CP Ti.

The comparison of resistance measurements and SEM observations is less convincing in Ti-6Al-7Nb alloy than in CP Ti. The microstructure remains unchanged after annealing up to 440**°C**, which is consistent with the resistance measurements. Despite resistance evolution suggests a microstructural transformation in the condition annealed to 550**°C**, no obvious microstructure changes were observed. On the other hand, other authors reported recovery process (identified by X-ray diffraction) and even the beginning of recrystallization (observed by TEM) in Ti-6Al-7Nb alloy prepared by ECAP and annealed at 500**°C** for 1 h [33]. However, our sample heated up to 550**°C** at a constant rate of 5**°C** min^{-1} was in fact exposed to temperatures above 500**°C** only for 10 min. This relatively short time of exposure to temperatures above 500**°C** might be insufficient for recovery process to be observed by SEM. Partially recrystallized structure of the sample annealed up to 660**°C** is shown in **Figure 6(d)** and is consistent with the results in Ref. [33], in which resistance measurements and observations of the similar UFG material annealed at 600**°C** for 1 h are reported. Therefore, we are convinced that electrical resistance measurement captured the recovery and recrystallization processes also in Ti-6Al-7Nb, despite the beginning of the process could not be unambiguously proven by SEM observations.

5. Conclusion

Evolution of microstructure of ultra-fine grained magnesium alloy AZ31, CP Ti (Grade 4), and Ti-6Al-7Nb alloy prepared by equal-channel angular pressing was investigated. Several experimental techniques were employed in order to identify the processes operating during heating of the material. The following conclusions can be drawn from this study:

- Ultra-fine grained titanium and magnesium-based materials were successfully prepared by ECAP. Microstructural refinement significantly increases their microhardness.
- UFG AZ31 alloy is stable up to 170°C (0.5 T_m), while CP Ti and Ti-6Al-7Nb alloy are stable approximately to 500°C, which corresponds to 0.4 T_m.
- The decrease of the microhardness upon annealing of both AZ31 alloy and CP Ti was attributed to annihilation of dislocation and subsequent grain growth.
- Recovery processes in Ti-6Al-7Nb alloy occur in the similar temperature range as in CP Ti. However, Ti-6Al-7Nb does not exhibit strong decrease of microhardness even after heating to 660°C, which is associated with solid solution strengthening of the material by phase interfaces.
- *In-situ* electrical resistance measurement is capable to detect recovery and/or recrystallization processes. It revealed differences in resistance evolution between ultra-fine grained and coarse grained condition of Ti-based materials. These differences correspond to microstructural changes observed by SEM and associated microhardness decrease.
- The kinetics of grain growth of AZ31 alloy was described by the Arrhenius equation and the activation energies of grain growth were determined. The values of activation energy continuously increase with increasing temperature due to changes of dominant diffusion mechanisms.

Acknowledgements

This work was financially supported by ERDF under the project "Nanomaterials centre for advanced applications," project No. CZ.02.1.01/0.0/0.0/15_003/0000485. J. Stráská also acknowledges Czech Science Foundation under the project 16-08963S. J. Stráský, K. Václavová, and P. Zháňal acknowledge Czech Science Foundation under the project 17-20700Y.

Author details

Jitka Stráská[1]*, Pavel Zháňal[1], Kristína Václavová[1], Josef Stráský[1], Petr Harcuba[1], Jakub Čížek[2] and Miloš Janeček[1]

*Address all correspondence to: straska.jitka@gmail.com

1 Department of Physics of Materials, Charles University, Prague, Czech Republic

2 Department of Low-Temperature Physics, Charles University, Prague, Czech Republic

References

[1] Gupta M, Sharon NML. In: Magnesium, Magnesium Alloys, and Magnesium Composites. New Jersey: John Wiley & Sons, Inc.; 2011. pp. 1-3

[2] Geetha M, Singh AK, Askomanani R, Gugia AK. Ti based biomaterials, the ultimate choice for orthopaedic implants—Review. Progress in Materials Science. 2009;**54**:397-425. DOI: 10.1016/j.pmatsci.2008.06.004

[3] Long M, Rack HJ. Titanium alloys in total joint replacement—A materials science perspective. Biomaterials. 1998;**19**:1621. DOI: 10.1016/S0142-9612(97)00146-4

[4] Elias CN, Meyers MA, Valiev RZ, Monteiro SN. Ultrafine grained titanium for biomedical applications: An overview of performance. Journal of Materials Research and Technology. 2013;**2**:340-350. DOI: 10.1016/j.jmrt.2013.07.003

[5] Welsch G, Boyer R, Collings EW, editors. Materials Properties Handbook: Titanium Alloys. ASM International, Materials Park, Ohio 44073-0002, USA; 1993

[6] Eisenbarth E, Velten D, Müller M, Thull R, Breme J. Biocompatibility of β-stabilizing elements of titanium alloys. Biomaterials. 2004;**25**:5705-5713. DOI: 10.1016/j.biomaterials.2004.01.021

[7] Yu J, Zhao ZJ, Li LX. Corrosion fatigue resistances of surgical implant stainless steel and titanium alloys. Corrosion Science. 1993;**35**:587-591. DOI: 10.1016/0010-938X(93)90193-K

[8] Leyens C, Peters M. Titanium and Titanium Alloys. Weinheim: Wiley-VCH; 2003. p. 2. DOI: 10.1002/3527602119

[9] Janeček M, Stráský J, Čížek J, Harcuba P, Václavová K, Polyakova VV, Semenova IP. Mechanical properties and dislocation structure evolution in Ti6Al7Nb alloy processed by high pressure torsion. Metallurgical and Materials Transactions A. 2014;**45A**:7-15. DOI: 10.4028/www.scientific.net/MSF.667-669.943

[10] Polyakova VV, Anumalasetty VN, Semenova IP, Valiev RZ. Influence of UFG structure formation on mechanical and fatigue properties in Ti-6Al-7Nb alloy. IOP Conference Series: Materials Science and Engineering. 2014;**63**:1-8. DOI: 10.1088/1757-899X/63/1/012162

[11] Valiev RZ, Islamgaliev RK, Alexandrov IV. Bulk nanostructured materials from severe plastic deformation. Progress in Materials Science. 2000;**45**:103-189. DOI: 10.1016/S0079-6425(99)00007-9

[12] Langdon TG. Twenty-five years of ultrafine-grained materials: Achieving exceptional properties through grain refinement. Acta Materialia. 2013;**61**:7035-7059. DOI: 10.1016/j.actamat.2013.08.018

[13] Valiev RZ, Estrin Y, Horita Z, Langdon TG, Zehetbauer MJ, Zhu YT. Producing bulk ultrafine-grained materials by severe plastic deformation. Journal of Management. 2006;**58**:33-39. DOI: 10.1007/s11837-006-0213-7

[14] Valiev RZ, Langdon TG. Principles of equal-channel angular pressing as a processing tool for grain refinement. Progress in Materials Science. 2006;**51**:881-981. DOI: 10.1016/j.pmatsci.2006.02.003

[15] Matsubara K, Miyahara Y, Horita Z, Langdon TG. Developing superplasticity in a magnesium alloy through a combination of extrusion and ECAP. Acta Materialia. 2003;**51**:3073-3084. DOI: 10.1016/S13596454(03)00118-6

[16] Zhilyaev AP, Langdon TG. Using high-pressure torsion for metal processing: Fundamentals and applications. Progress in Materials Science. 2008;**53**:893-979. DOI: 10.1016/j.pmatsci.2008.03.002

[17] Saito Y, Utsunomiya H, Tsuji N, Sakai T. Novel ultra-high straining process for bulk materials—Development of the accumulative roll-bonding (ARB) process. Acta Materialia. 1999;**47**:579-583. DOI: 10.1016/S1359-6454(98)00365-6

[18] Horita Z, Fujinami T, Langdon TG. The potential for scaling ECAP: Effect of sample size on grain refinement and mechanical properties. Materials Science and Engineering: A. 2001;**318**:34-41. DOI: 10.1016/S0921-5093(01)01339-9

[19] Agnew SR, Horton JA, Lillo TM, Brown DW. Enhanced ductility in strongly textured magnesium produced by equal channel angular processing. Scripta Materialia. 2004;**50**:377-381. DOI: 10.1016/j.scriptamat.2003.10.006

[20] Janeček M, Popov M, Krieger MG, Hellmig RJ, Estrin Y. Mechanical properties and microstructure of a Mg alloy AZ31 prepared by equal-channel angular pressing. Materials Science and Engineering: A. 2007;**462**:116-120. DOI: 10.1016/j.msea.2006.01.174

[21] Figueiredo RB, Langdon TG. Developing superplasticity in a magnesium AZ31 alloy by ECAP. Journal of Materials Science. 2008;**43**:7366-7371. DOI: 10.1007/s1085-008-2846-0

[22] Figueiredo RB, Langdon TG. Grain refinement and mechanical behavior of a magnesium alloy processed by ECAP. Journal of Materials Science. 2010;**45**:4827-4836. DOI: 10.1007/s10853-010-4589-y

[23] Xu J, Shirooyeh M, Wongsa-Ngam J, Shan D, Guo B, Langdon TG. Hardness homogeneity and micro-tensile behavior in a magnesium AZ31 alloy processed by equal-channel angular pressing. Materials Science and Engineering: A. 2013;**586**:108-114. DOI: 10.1016/j.msea.2013.07.096

[24] Stolyarov VV, Zhu YT, Lowe TC, Islamgaliev RK, Valiev RZ. A two-step SPD processing of ultrafine-grained titanium. Nanostructured Materials. 1999;**11**:947-954. DOI: 10.1016/S0965-9773(99)00384-0

[25] Islamgaliev RK, Kazyhanov VI, Shestakova LI, Sharafurdinov AV, Valiev RZ. Microstructure and mechanical properties of titanium (Grade 4) processed by high-pressure torsion. Materials Science and Engineering: A. 2008;**493**:190-194. DOI: 10.1016/j.msea.2007.08.084

[26] Wang YC, Langdon TG. Influence of phase volume fractions on the processing of a Ti-6Al-4V alloy by high-pressure torsion. Materials Science and Engineering: A. 2013;**559**:861-867. DOI: 10.1016/j.msea.2012.09.034

[27] Gubicza J, Chinh NQ, Dobatkin SV, Khosravi E, Langdon TG. Stability of ultrafine-grained microstructure in fcc metals processed by severe plastic deformation. Key Engineering Materials 2011;**465**:195-198. DOI: 10.4028/www.scientific.net/KEM.465.195

[28] Kim HK. Activation energies for the grain growth of an AZ31 Mg alloy after equal channel angular pressing. Journal of Materials Science (Letters). 2004;**39**:7107-7109. DOI: 10.1023/B:JMSC.0000047560.93940.45

[29] Radi Y, Mahmudi R. Effect of Al_2O_3 nano-particles on the microstructural stability of AZ31 Mg alloy after equal channel angular pressing. Materials Science and Engineering: A. 2010;**527**:2764-2771. DOI: 10.1016/j.msea.2010.01.029

[30] Vrátná J, Janeček M, Čížek J, Lee DJ, Yoon EY, Kim HS. Mechanical properties and microstructure evolution in ultrafine-grained AZ31 alloy processed by severe plastic deformation. Journal of Materials Science. 2013;**48**:4705-4712. DOI: 10.1007/s10853-013-7151-x

[31] Zháňal P, Václavová K, Hadzima B, Harcuba P, Stráský J, Janeček M, Polyakova V, Semenova I, Hájek M, Hajizadeh K. Thermal stability of ultrafine-grained commercial purity Ti and Ti–6Al–7Nb alloy investigated by electrical resistance, microhardness and scanning electron microscopy. Materials Science and Engineering: A. 2016;**651**:886-892. DOI: 10.1016/j.msea.2015.11.029

[32] Hajizadeh K, Eghbali B, Topolski K, Kurzydlowski KJ. Ultra-fine grained bulk CP-Ti processed by multi-pass ECAP at warm deformation region. Materials Chemistry and Physics. 2014;**143**:1032-1038. DOI: 10.1016/j.matchemphys.2013.11.001

[33] Polyakova V, Semenova IP, Valiev RZ. Influence of annealing on the structure and mechanical properties of ultrafine-grained alloy Ti–6Al–7Nb, processed by severe plastic deformation. Materials Science Forum. 2010;**667-669**:943-948. DOI: 10.4028/www.scientific.net/MSF.667-669.943

[34] Hájek M, Veselý J, Cieslar M. Precision of electrical resistivity measurements. Materials Science and Engineering: A. 2007;**462**:339-342. DOI:10.1016/j.msea.2006.01.175

[35] Vrátná J, Janeček M. Experimental study of ultrafine-grained commercial magnesium alloy AZ31 prepared by severe plastic deformation. In: Proceeding of the 22st International Conference on Metallurgy and Material (METAL 2013). 2014. ISBN 978-80-87294-39-0

[36] Stráská J, Janeček M, Čížek J, Stráský J, Hadzima B. Microstructure stability of ultrafine grained magnesium alloy AZ31 processed by extrusion and equal-channel angular pressing (EX–ECAP). Materials Characterization. 2014;**94**:69-79. DOI: 10.1016/j.matchar.2014.05.013

[37] Aghababaei R, Joshi SP. Micromechanics of tensile twinning in magnesium gleaned from molecular dynamics simulations. Acta Materialia. 2014;**69**:326-342. DOI: 10.1016/j.actamat.2014.01.014

[38] Kazemi-Choobi K, Khalil-Allafi J, Abbasi-Chianeh V. Investigation of the recovery and recrystallization processes of Ni50.9Ti49.1 shape memory wires using in situ electrical resistance measurement. Materials Science and Engineering: A. 2012;**551**:122-127. DOI: 10.1016/j.msea.2012.04.106

[39] Stráská J, Stráský J, Minárik P, Janeček M, Hadzima B. Continuous measurement of *m*-parameter for analyzing plastic instability in a superplastic ultra-fine grained magnesium alloy. Materials Science and Engineering: A. 2017;**684**:110-114. DOI: 10.1016/j.msea.2016.12.027

[40] Huang Y, Langdon TG. Characterization of deformation processes in a Zn-22% Al alloy using atomic force microscopy. Journal of Materials Science. 2002;**37**:4993-4998. DOI: 10.1023/A:1021071228521

[41] Vinogradov A, Hashimoto S, Patlan V, Kitagawa K. Atomic force microscopic study on surface morphology of ultra-fine grained materials after tensile testing. Materials Science and Engineering: A. 2001;**319-321**:862-866. DOI: 10.1016/S0921-5093(01)01057-7

[42] Han JH, Mohamed FA. Quantitative measurements of grain boundary sliding in an ultrafine-grained Al alloy by atomic force microscopy. Metallurgical and Materials Transactions A. 2011;**42**:3969-3978. DOI: 10.1007/s11661-011-0871-0

[43] Estrin Y, Tóth LS, Molinari A, Bréchet Y. A dislocation-based model for all hardening stages in large strain deformation. Acta Materialia. 1998;**46**:5509-5522. DOI: 10.1016/S1359-6454(98)00196-7

[44] Hall EO. The deformation and ageing of mild steel: III discussion of results. Proceedings of the Royal Society. 1951;**B64**:747-753. DOI: 10.1088/0370-1301/64/9/303

[45] Petch NJ. The cleavage strength of polycristals. The Journal of the Iron and Steel Institute. 1953;**174**:25-27

[46] Higgins GT. Grain-boundary migration and grain growth. Metal Science. 1974;**8**:143-150

[47] Kim HK, Kim WJ. Microstructural instability and strength of an AZ31 Mg alloy after severe plastic deformation. Materials Science and Engineering: A. 2004;**385**:300-308. DOI: 10.1016/j.msea.2004.06.055

[48] Cao P, Lu L, Lai MO. Grain growth and kinetics for nanocrystalline magnesium alloy produced by mechanical alloying. Materials Research Bulletin. 2001;**36**:981-988. DOI: 10.1016/S0025-5408(01)00578-5

[49] Thein MA, Lu L, Lai MO. Kinetics of grain growth in nanocrystalline magnesium-based metal–metal composite synthesized by mechanical alloying. Composites Science and Technology. 2006;**66**:531-537. DOI: 10.1016/j.compscitech.2005.07.002

[50] Miao Q, Hu L, Wang X, Wang E. Grain growth kinetics of a fine-grained AZ31 magnesium alloy produced by hot rolling. Journal of Alloys and Compounds. 2010;**493**:87-90. DOI: 10.1016/j.jallcom.2009.12.049

[51] Chao HY, Sun HF, Chen WZ, Wang ED. Static recrystallization kinetics of a heavily cold drawn AZ31 magnesium alloy under annealing treatment. Materials Characterization. 2011;**62**:312-320. DOI: 10.1016/j.matchar.2011.01.007

[52] Frost HJ, Ashby MF. Deformation-Mechanism Maps. Oxford: Pergamon Press; 1982. pp. 43-45

[53] Shewman PG. Self-diffusion in Mg single crystals. Trans AIME. 1956;**206**:918-22

[54] Wang J, Iwahashi Y, Horita Z, Furukawa M, Nemoto M, Valiev RZ, Langdon TG. An investigation of microstructural stability in an AlMg alloy with submicrometer grain size. Acta Materialia. 1996;**44**:2973-2982. DOI: 10.1016/1359-6454(95)00395-9

[55] Valiev RZ, Kozlov EV, Ivanov YF, Lian J, Nazarov AA, Baudelet B. Deformation behaviour of ultra-fine-grained copper. Acta Metallurgica et Materialia. 1994;**42**:2467-2475. DOI: 10.1016/0956-7151(94)90326-3

[56] Lian J, Valiev RZ, Baudelet B. On the enhanced grain growth in ultrafine grained metals. Acta Metallurgica et Materialia. 1995;**43**:4165-4170. DOI: 10.1016/0956-7151(95)00087-C

[57] Janeček M, Yi S, Král R, Vrátná J, Kainer KU. Texture and microstructure evolution in ultrafine-grained AZ31 processed by EX-ECAP. Journal of Materials Science. 2010;**45**:4665-4671. DOI: 10.1007/s10853-010-4675-1

[58] Stráská J, Stráský J, Janeček M. Activation energy for grain growth of the isochronally annealed ultrafine grained magnesium alloy after hot extrusion and equal-channel angular pressing (EX-ECAP). Acta Physica Polonica A. 2015;**128**:578-581

[59] Furukawa M, Horita Z, Nemoto M, Valiev RZ. Microhardness measurements and the Hall-Petch relationship in an Al+Mg alloy with submicrometer grain size. Acta Materialia. 1996;**51**:4619-4629. DOI: 10.1016/1359-6454(96)00105-X

[60] Vrátná J, Janeček M, Stráský J, Kim HS, Yoon EY. Investigation of microhardness and microstructure of AZ31 alloy after high pressure torsion. Magnesium Technology, Magnesium Technology Series. 2011:589-594

[61] Lin HK, Huang JC. High strain rate and/or low temperature superplasticity in AZ31 Mg alloys processed by simple high-ratio extrusion methods. Materials Transactions. 2002;**43**:2424-2432

[62] Lin HK, Huang JC, Langdon TG. Relationship between texture and low temperature superplasticity in an extruded AZ31 Mg alloy processed by ECAP. Materials Science and Engineering: A. 2005;**402**:250-257. DOI: 10.1016/j.msea.2005.04.018

[63] Figueiredo RB, Langdon TG. Principles of grain refinement and superplastic flow in magnesium alloys processed by ECAP. Materials Science and Engineering: A. 2009;**501**:105-114. DOI: 10.1016/j.msea.2008.09.058

[64] Mohan A, Yuan W, Mishra RS. High strain rate superplasticity in friction stir processed ultrafine grained Mg-Al-Zn alloys. Materials Science and Engineering: A. 2013;**562**:69-76. DOI: 10.1016/j.msea.2012.11.026

[65] Janeček M, Čížek J, Gubicza J, Vrátná J. Microstructure and dislocation density evolutions in MgAlZn alloy processed by severe plastic deformation. Journal of Materials Science. 2012;**47**:7860-7869. DOI: 10.1007/s10853-012-6538-4

[66] Young JP, Askari H, Hovanski Y, Heiden MJ, Field DP. Thermal microstructural stability of AZ31 magnesium after severe plastic deformation. Materials Characterization. 2015;**101**:9-19. DOI: 10.1016/j.matchar.2014.12.026

[67] Langdon TG. The mechanical properties of superplastic materials. Metallurgical and Materials Transactions A. 1982;**13**:689-701. DOI: 10.1007/BF02642383

[68] Cormier M, Claisse F. Composition dependence of the thermal coefficient of electrical resistivity of c.p.h. titanium-oxygen alloys. Journal of the Less Common Metals. 1976;**48**:309-314. DOI: 10.1016/0022-5088(76)90010-2

[69] Powell RW, Tye RP. The thermal and electrical conductivity of titanium and its alloys. Journal of the Less Common Metals. 1961;**48**:309-314. DOI: 10.1016/0022-5088(61)90064-9

[70] Malinov S, Markovsky P, Sha W, Guo Z. Resistivity study and computer modelling of the isothermal transformation kinetics of Ti-6Al-4V and Ti-6Al-2Sn-4Zr-2Mo-0.08Si alloys. Journal of Alloys and Compounds. 2001;**314**:181-192. DOI: 10.1016/S0925-8388(00)01227-5

[71] Welsch G, Lütjering G, Gazioglu K, Bunk W. Deformation characteristics of age hardened Ti-6Al-4V. Metallurgical and Materials Transactions A. 1977;**8**:169-177. DOI: 10.1007/BF02677278

[72] Guo S, Meng Q, Liao G, Zhao X. Microstructural evolution and mechanical behaviour of metastable β-type Ti-25Nb-2Mo-4Sn alloy with high strength and low modulus. Progress in Natural Science: Materials. 2013;**23**:174-182. DOI: 10.1016/j.pnsc.2013.03.008

[73] Hoseini M, Pourian MH, Bridier F, Vali H, Szpunar JA, Bocher P. Thermal stability and annealing behaviour of ultrafine commercially pure titanium. Materials Science and Engineering: A. 2012;**532**:58-63. DOI: 10.1016/j.msea.2011.10.062

IntechOpen

IntechOpen